JGR Oceans

RESEARCH ARTICLE
10.1029/2020JC016066

On the Generation and Salinity Impacts of Intraseasonal Westward Jets in the Equatorial Indian Ocean

Ebenezer S. Nyadjro[1,2], Adam V. Rydbeck[3], Tommy G. Jensen[3], James G. Richman[4], and Jay F. Shriver[3]

[1]Department of Physics, University of New Orleans, New Orleans, LA, USA, [2]Now at Northern Gulf Institute, Mississippi State University, Stennis Space Center, MS, USA, [3]Naval Research Laboratory, Stennis Space Center, MS, USA, [4]Center for Ocean-Atmospheric Prediction Studies, Florida State University, Tallahassee, FL, USA

Key Points:
- Intraseasonal equatorial westward jet anomalies in the Indian Ocean are generated and terminated by local intraseasonal surface winds
- Barrier layer thickness increases following the passage of westward jets
- Intraseasonal westward jets freshen the equatorial mixed layer through zonal advection

Correspondence to:
E. S. Nyadjro,
esn31@msstate.edu

Citation:
Nyadjro, E. S., Rydbeck, A. V., Jensen, T. G., Richman, J. G., & Shriver, J. F. (2020). On the generation and salinity impacts of intraseasonal westward jets in the equatorial Indian Ocean. *Journal of Geophysical Research: Oceans*, *125*, e2020JC016066. https://doi.org/10.1029/2020JC016066

Received 8 JAN 2020
Accepted 21 MAY 2020
Accepted article online 27 MAY 2020

Abstract While westerly winds dominate the equatorial Indian Ocean and generate the well-known eastward flowing Wyrtki Jets during boreal spring and fall, there is evidence of a strong westward surface jet during winter that is swifter than eastward currents during that season. A weaker westward jet is found in summer. In this study, we report the occurrence, characteristics, and intraseasonal variability of this westward jet and its impact on mixed layer salinity in the equatorial Indian Ocean using the HYbrid Coordinate Ocean Model (HYCOM) reanalysis with the Navy Coupled Ocean Data Assimilation (NCODA). The westward jet typically occurs in the upper 50 m, above an eastward flowing equatorial undercurrent, with peak westward volume transport of approximately −8 Sv. The westward jet builds up gradually, decays rapidly, and is primarily forced by local intraseasonal wind stress anomalies generated by atmospheric intraseasonal convection. Westward acceleration of the jet occurs when the dominant intraseasonal westward wind anomaly is not balanced by the zonal pressure gradient (ZPG) force. The intraseasonal westward jet generates strong horizontal advection and is the leading cause of mixed layer freshening in the western equatorial Indian Ocean. Without it, a saltier mixed layer would persist and weaken any barrier layers. Existing barrier layers are strengthened following the passage of freshwater-laden westward jets. Deceleration of the westward jet occurs when the eastward ZPG becomes increasingly important and the westward intraseasonal wind anomalies weaken. A rapid reversal of atmospheric intraseasonal convection-driven surface winds eventually terminates the westward jet.

Plain Language Summary This study investigates currents that flow and travel from east to west along the equator in the Indian Ocean. We examine potential mechanisms of current variability using a reanalysis version of the global HYbrid Coordinate Ocean Model (HYCOM). The Indian Ocean experiences seasonal wind reversals, which drive much of the surface ocean dynamics. Our results show that the winds vary more frequently than the currents. These intraseasonal winds are the main causes of intense westward currents. The westward jet is stronger during winter than summer, a likely result of winds persisting for a longer time during winter than during summer. Strong intraseasonal westward currents transport freshwater from the east to the central and western Indian Ocean. Rapid reversal of the intraseasonal winds from westward to eastward causes the surface currents to reverse direction from westward to eastward.

1. Introduction

Intraseasonal surface zonal current variability in the equatorial Indian Ocean is dominated by the Yoshida-Wyrtki jets (Wyrtki, 1973; Yoshida, 1959) forced by intraseasonal oscillations (ISOs) (Madden & Julian, 1971). Seasonal wind-driven currents are eastward flowing during the Indian intermonsoon periods: the boreal spring during April–May and the boreal fall during October–November. Many previous studies (e.g., Han et al., 1999; Jensen, 1993; Knox, 1976; Nyadjro & McPhaden, 2014) have focused on the dynamics of the eastward zonal surface current variability in the equatorial Indian Ocean and showed that these currents are typically strong and can exceed 1.2 m s^{-1} (Figure 1b). During boreal summer and winter, however, equatorial surface currents weaken and/or reverse becoming westward flowing (Figure 1; Han et al., 1999; Joseph et al., 2012; Rydbeck et al., 2017). There are limited studies on the intraseasonal variability (ISV) of westward surface currents, even though they modulate the exchange of heat, momentum, and salt, across the tropical Indian Ocean (Cane, 1980; Nagura & McPhaden, 2008; Rydbeck et al., 2017). In order to

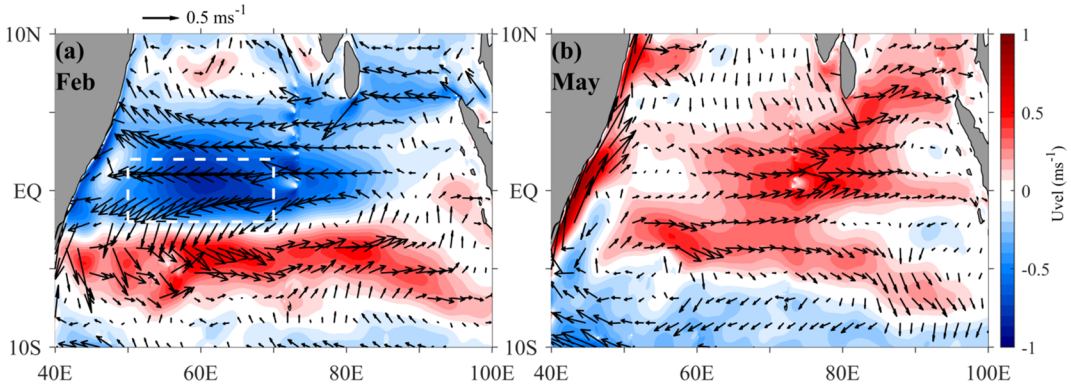

Figure 1. Mean zonal current (color shading, m s^{-1}) and currents (vectors, m s^{-1}) for (a) February and (b) May. White box in Figure 1a, 50–70°E, 2°S to 2°N, shows the region where westward jets tend to be strongest.

construct a complete understanding of intraseasonal surface current variability in the equatorial Indian Ocean, we identify the salient features of the Yoshida-Wyrtki jet's counterpart, the westward jet (Figure 1a).

Many studies on zonal currents in the equatorial Indian Ocean focus on the semiannual (Luyten & Roemmich, 1982; Nagura & McPhaden, 2010; Wyrtki, 1973), seasonal (e.g., Han et al., 1999; Rao et al., 1989), and interannual (e.g., Gnanaseelan et al., 2012; Joseph et al., 2012; McPhaden et al., 2015; Nyadjro & McPhaden, 2014) variability with relatively few studies on ISV. Much of the research attention is on the impact of winds associated with the seasonal monsoon and the dominant interannual modes of variability, such as the Indian Ocean Dipole (IOD) and El Niño Southern Oscillation (ENSO), on surface currents. However, it has been noted that intraseasonal variations of zonal currents in the equatorial Indian Ocean can be as large as the seasonal variations (Senan et al., 2003). Cane (1980) observed a local and rapid response of the equatorial currents to westerly and meridional winds at 73°E. Luyten and Roemmich (1982) reported a dominant 30- to 60-day variability of zonal currents in the upper 200 m in the western equatorial Indian Ocean. Rydbeck et al. (2017) observed that intraseasonal westward jets warm the sea surface in the western Indian Ocean by advecting the climatological Indian Ocean warm pool westward. They also observed that the zonal extent of the westward jet was approximately one half the wavelength of the first baroclinic mode equatorial Rossby waves, whereas the Wyrtki jet extends across most of the equatorial Indian Ocean (Delcroix et al., 1991; Jensen, 1993).

While both the eastward and westward jets are forced primarily as a response to local winds (Cane, 1980), there are however differences in their structures and occurrences. The westward jets are shallower, typically occurring in the upper 50 m (Figure 2c). Temporally, the westward jets tend to occur during boreal winter and summer (albeit weaker than the winter occurrence; Figures 1a and 2a).

The eastward jets on the other hand are deeper, occurring in the upper 80–100 m (Han et al., 1999; Iskandar & McPhaden, 2011; Nyadjro & McPhaden, 2014). They tend to occur during the intermonsoon periods earlier mentioned (Figure 1b). Observed differences in the strength of the spring eastward jet and the fall eastward jet vary in the literature. Studies by Han et al. (1999) and Qiu et al. (2009) suggest that the climatological Wyrtki jet is stronger during boreal fall than during boreal spring. Gnanaseelan et al. (2012) however reported the opposite, but results from Nagura and McPhaden (2010) and Nyadjro and McPhaden (2014) suggest both fall and spring jets to be of approximately similar magnitudes. Summarily, the characteristics of westward jets and their impacts are quite different from eastward-flowing Wyrtki jets along the equatorial Indian Ocean, prompting further investigation.

ISV of ocean currents is fundamentally generated by resonant winds (Figure 3; Sengupta et al., 2001). The ISO of equatorial Indian Ocean winds manifests as the boreal summer intraseasonal oscillation (BSISO) during Northern Hemisphere summer and the Madden-Julian Oscillations (MJO) (Madden & Julian, 1971) during winter. The ISO, a coupled ocean-atmosphere phenomena that typically occurs on 40- to 50-day periods, impacts SST, precipitation, and the atmospheric circulation. It has also been observed to rectify onto phenomena with longer timescales such as ENSO and IOD (DeMott et al., 2015; Deshpande et al., 2017;

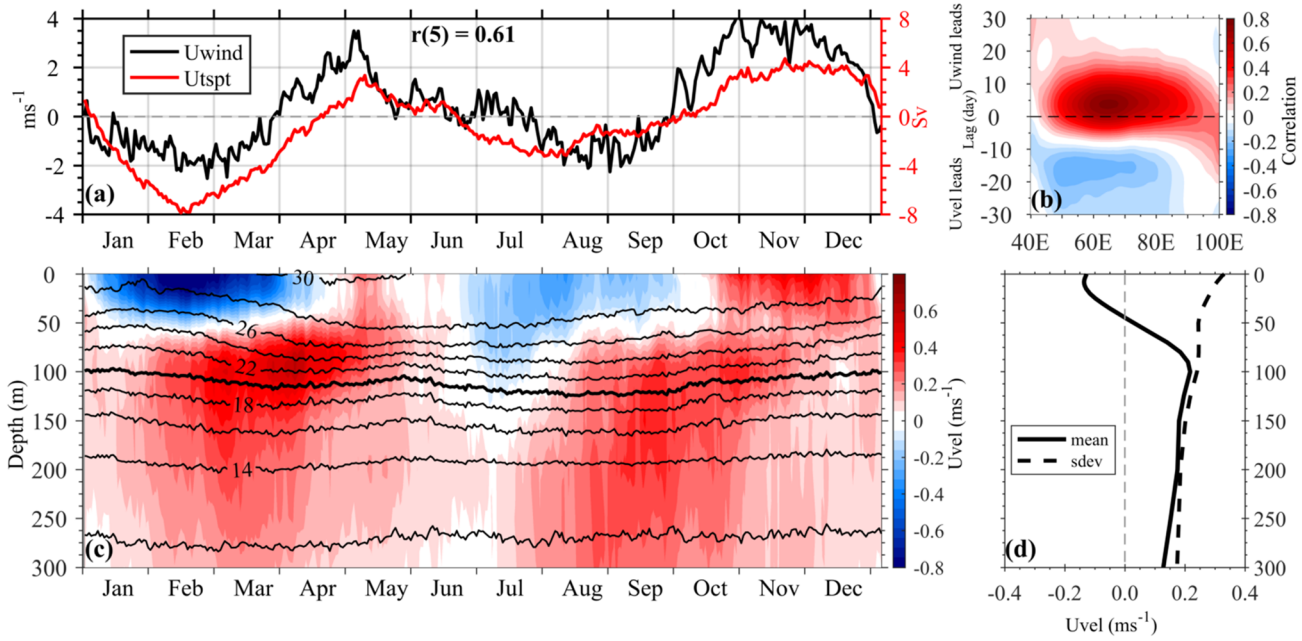

Figure 2. (a) Daily climatology of zonal winds (black line, m s^{-1}) and zonal volume transport (red line, Sv) box-averaged in the western equatorial Indian Ocean (i.e., white box in Figure 1a). The strongest correlation between winds and transport (0.61) occurs when the winds lead the currents by about 5 days. (b) Lead-lag correlations of box-averaged intraseasonal zonal wind anomalies and zonal current anomalies in the western Indian Ocean. (c) Daily climatology of box-averaged zonal currents in the upper 300 m in the western Indian Ocean from HYCOM (color shading, m s^{-1}). Contours show temperature climatology (°C). The thermocline depth represented by the 20°C isotherm is highlighted. (d) Box-averaged annual mean zonal currents (solid black line, m s^{-1}) and standard deviation of intraseasonal current anomalies (dashed black line, m s^{-1}) in the upper 300 m in the western Indian Ocean.

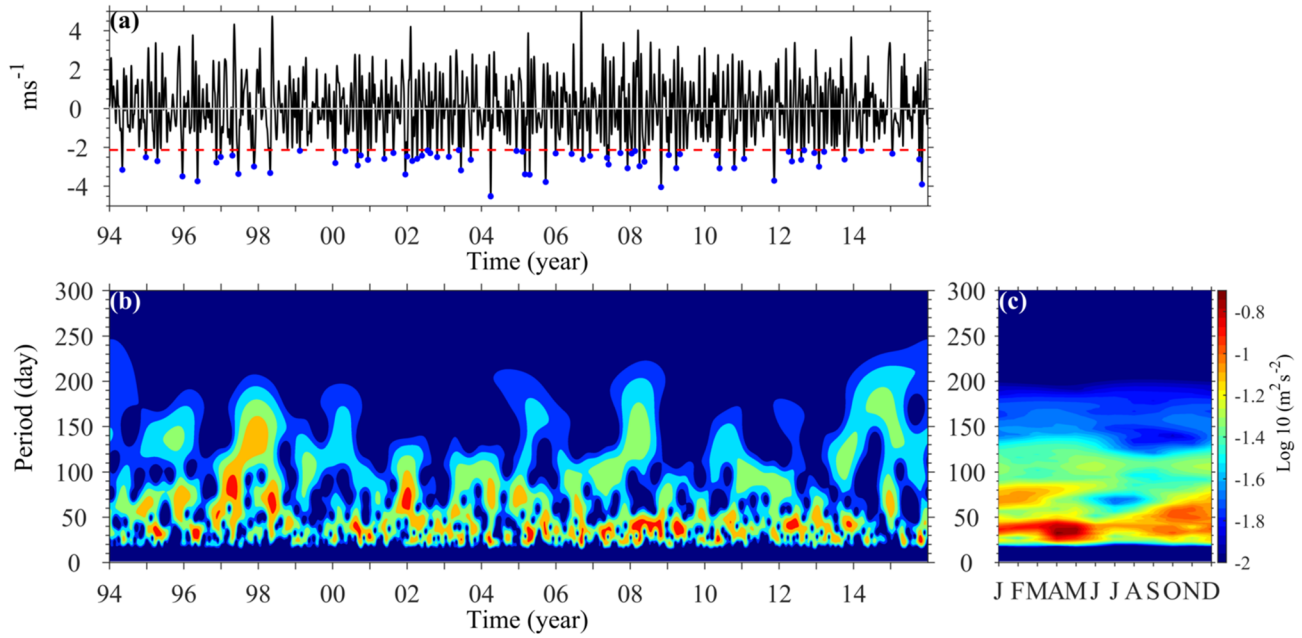

Figure 3. (a) Intraseasonal anomalies of zonal winds (m s^{-1}) averaged in the western Indian Ocean (i.e., white box in Figure 1b). Red line shows 1.5 standard deviations of the filtered, intraseasonal anomalies. Blue dots indicate the westward zonal current events as defined in section 2. (b) Wavelet power spectrum (WPS) of filtered anomalous zonal winds in the western Indian Ocean. (c) Climatology of the WPS.

Hendon et al., 1999). Low-level winds associated with the ISO accelerate surface zonal currents in the equatorial Indian Ocean. On select occasions, ISO-forced equatorial Rossby waves generate westward jets that transport warm water to the western Indian Ocean and aid the onset of subsequent MJO events (Rydbeck et al., 2017).

Aside from forcing ISVs of ocean currents, atmospheric ISOs generate variability of salinity in the upper ocean, affecting ocean stratification, which can subsequently feedback onto ISO convection (DeMott et al., 2015; Drushka et al., 2014; Grunseich et al., 2011). On intraseasonal time scales, sea surface salinity (SSS) in the Indian Ocean varies by ~0.2 psu and is controlled by freshwater flux (evaporation minus precipitation), advection, and mixing (Grunseich et al., 2013; Matthews et al., 2010). The relative contributions by these processes to intraseasonal SSS variability vary by location and phases of the atmospheric ISOs. Li et al. (2015) suggest that wind-driven ocean dynamical processes are the primary cause of SSS ISV in most of the equatorial Indian Ocean with freshwater fluxes playing a secondary role. During the active phase of the ISO, however, enhanced precipitation is the primary contributor and causes low-salinity anomalies in the Indian Ocean (Grunseich et al., 2011). Anomalous winds associated with the ISO force intraseasonal jets that advect these low salinity anomalies along the equator (Drushka et al., 2014). The importance of horizontal advection to the intraseasonal salt budget in the western equatorial Indian Ocean has not been previously explored.

The western equatorial Indian Ocean is a region of economic and climatic importance. It is biologically productive and supports a large fishery (Liao et al., 2017), with the variability and distribution of chlorophyll (a key component of this productivity) impacted by surface currents (McCreary et al., 2009). The temperature-influenced vertical stratification in the western equatorial Indian Ocean makes the region susceptible to significant air-sea interactions (Hermes & Reason, 2008; Nyadjro et al., 2017; Trenary & Han, 2012). Despite the dominant temperature influence, salinity has been suggested to further enhance the vertical ocean stratification in the western Indian Ocean (Chowdary et al., 2009; D'Addezio & Subrahmanyam, 2016), hence requiring further investigation.

In this study, we use observations and the HYbrid Coordinate Ocean Model (HYCOM) reanalysis that utilizes the Navy Coupled Ocean Data Assimilation (NCODA) to characterize the occurrence, evolution, features, and ISV of the westward surface jets in the equatorial Indian Ocean. We also examine the role of the jet in modulating intraseasonal mixed layer salinity anomalies.

2. Data and Methods

2.1. Data

Daily gridded 0.75° × 0.75° ocean surface winds are obtained from the European Centre for Medium-Range Weather Forecasts (ECMWF) reanalysis (Dee et al., 2011). Outgoing Longwave Radiation (OLR; used as a proxy for atmospheric convection) data on a 2.5° × 2.5° grid is obtained from the National Oceanic and Atmospheric Administration (NOAA) (Liebmann & Smith, 1996).

Daily averages of sea surface height (SSH), salinity, temperature, and currents from a reanalysis version of the HYCOM for January 1994 to December 2015 are used in this study. The dynamic model used is HYCOM configured for the global ocean with a nominal horizontal resolution of 1/12° (~8 km at the equator) and 41 hybrid vertical layers. The first 16 vertical layers are fixed in pressure (z level) and correspond to the upper 100 m, which ensures a good representation of mixed-layer processes (Metzger et al., 2017). The vertical coordinate is isopycnal in the open stratified ocean and approximately equal pressure levels (z levels) in the unstratified ocean. However, the model switches to a terrain-following (σ) coordinate in coastal waters via the layered continuity equation. HYCOM has the capability of selecting one of several different vertical mixing submodels (Halliwell, 2004), and this experiment uses the NASA Goddard Institute for Space Studies (GISS) Level 2 turbulence closure model (Canuto et al., 2001, 2002). The bathymetry is derived from the 30-arc second General Bathymetric Chart of the Oceans (GEBCO) data set (IOC, IHO, & BODC, 2003). Data assimilation is performed once a day using the NCODA (Cummings, 2005). NCODA assimilates available satellite altimeter and SST data in addition to in situ temperature and salinity data from conductivity-temperature-depth profiles, expandable bathythermograph profiles, Argo floats, and moored buoys through a 3-D variational scheme. The surface forcing is from the National Center for Environmental Prediction

(NCEP) Climate Forecast System Reanalysis (CFSR) wind, heat fluxes (computed using bulk formula), and precipitation fields (Saha et al., 2010).

2.2. Methods

We obtained ISV as in Rydbeck et al. (2017) by first removing the seasonal cycle and then applying a 20- to 200-day band-pass filter in order to isolate the ISV of interest. This choice of band-pass filtering window is to ensure that the slower response of the ocean to higher-frequency atmospheric intraseasonal forcing is captured. The 200-day low-frequency bound avoids the truncation of lower frequency oceanic ISV. For instance, this might include the second baroclinic mode Rossby wave response, which has a much lower frequency (~200 days) than the first mode (~90 days). We identify periods of strong westward jets in the western Indian Ocean by averaging intraseasonal zonal current anomalies from 2°N to 2°S and 50–70°E. This averaging box encompasses the core of the intraseasonal westward currents (Figures 1 and 2). It is also part of the region identified in Rydbeck et al. (2017) as an area in the western equatorial Indian Ocean where the zonal SST gradient maximizes (and stimulates air-sea interactions) as a result of westward advection of warm SST by equatorial Rossby waves. Using this averaging box also allows us to examine the contribution of salinity to stratification in the western equatorial Indian Ocean.

To characterize periods of robust westward jets, we identified strong westward jet events that are composited with filtered data to reveal salient features of their dynamics, temporal evolution of the zonal currents, wind forcing, OLR, salinity, and SSH. In this study, qualifying westward jet events are those that exceed 1.5 standard deviations of the area-averaged intraseasonal zonal current anomalies. From the HYCOM reanalysis, 45 westward jet events were identified from 1994–2015 (Figure 4a).

Volume transports are calculated from 2°N to 2°S, and down to 50 m depth. The meridional bounds of the calculation isolate the westward equatorial surface current from the south equatorial counter current (SECC). The vertical limit ensures that the calculation is performed over the surface westward current and is not impacted by the subsurface, eastward-flowing current that occurs in the thermocline region.

We computed the mixed layer depth (MLD) following the methods of de Boyer Montégut et al. (2004), which uses a variable density threshold equivalent to 0.2°C to define the MLD:

$$\Delta\sigma_\theta = \sigma_\theta(T_{10} - 0.2, S_{10}, P_0) - \sigma_\theta(T_{10}, S_{10}, P_0) \tag{1}$$

where $\Delta\sigma_\theta$ is the change in potential density between a reference depth (i.e., 10 dbar) and the base of the mixed layer. T_{10} and S_{10} are, respectively, temperature and salinity at 10 dbar, and P_0 is sea surface pressure.

We computed zonal momentum budget as in Drenkard and Karnauskas (2014) and Nagura and McPhaden (2014):

$$\left[\frac{\partial u}{\partial t}\right]' = -\left[u\frac{\partial u}{\partial x}\right]' - \left[v\frac{\partial u}{\partial y}\right]' - \left[w\frac{\partial u}{\partial z}\right]' - \left[\frac{1}{\rho}\frac{\partial p}{\partial x}\right]' + [fv]' + \left(\frac{\tau_o^x}{\rho}\right)' - \left(\frac{\tau_{ML}^x}{\rho}\right)' + \left[A_H\nabla^2 u\right]' \tag{2}$$

The square brackets represent vertical integration over the mixed layer. The primed terms are band-pass filtered for 20–200 days in order to obtain intraseasonal anomalies of each term. The terms are first computed using the total fields before filtering is applied. From left to right the terms in Equation 2 are the time rate of change in zonal velocity (i.e., zonal acceleration), zonal momentum advection, meridional momentum advection, vertical momentum advection, zonal pressure gradient (ZPG) force (computed as the residual from Equation 2), Coriolis force, surface wind stress, shear stress at the base of the mixed layer, and horizontal friction terms. u, v, and w are, respectively, zonal velocity, meridional velocity, and vertical velocity. p is pressure, ρ is density of sea water, and f is the Coriolis parameter. The surface wind stress, τ_o^x, is obtained from the 10-m wind speed, $\mathbf{U}$, using $\tau_o^x = \rho_a C_d |\mathbf{U}|\mathbf{U}$, where ρ_a is the density of air (1.225 kg m^{-3}) and C_d is a constant drag coefficient (1.43×10^{-3}; Weisberg & Wang, 1997). The shear stress at the mixed layer base τ_{ML}^x is computed as $\tau_{ML}^x = \rho A_V \frac{\partial u}{\partial z}$, where A_V is vertical viscosity (4.5×10^{-3} m^2 s^{-1}; Qiao & Weisberg, 1997). A_H is horizontal viscosity (1.5×10^3 m^2 s^{-1}; Wallcraft et al., 2005).

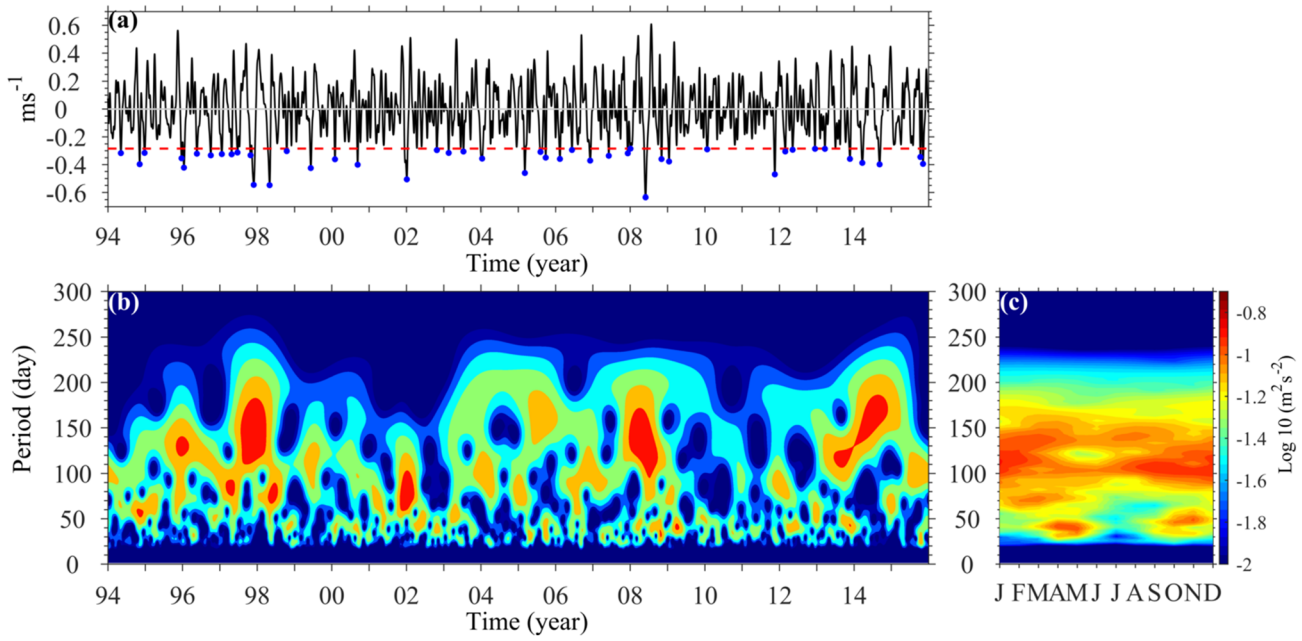

Figure 4. (a) Intraseasonal anomalies of zonal currents (m s^{-1}) averaged in the western equatorial Indian Ocean (i.e., white box in Figure 1b). Red line shows 1.5 standard deviations of the filtered, intraseasonal anomalies. Blue dots indicate the westward events as defined in the section 2. (b) Wavelet power spectrum (WPS) of filtered anomalous zonal currents in the western Indian Ocean. (c) Climatology of the WPS.

To better understand the impact of westward jets on salinity, contributions to the intraseasonal mixed layer salinity tendency are calculated using the following formula:

$$\left(\frac{\partial S}{\partial t}\right)' = \left(S\frac{E-P}{h}\right)' - \left(u\frac{\partial S}{\partial x}\right)' - \left(v\frac{\partial S}{\partial y}\right)' - \left(w_e\frac{\partial S}{\partial z}\right)' + R \tag{3}$$

From left to right, the terms in Equation 3 represent the mixed layer salinity tendency, sea surface freshwater forcing, zonal salt advection, meridional salt advection, interaction of mixed layer with the layer below, and the residual. S is the salinity vertically averaged over the MLD, h. E is evaporation, and P is precipitation, both obtained from the NCEP CFSR data set used to force the model. $\frac{\partial S}{\partial z}$ is computed as the difference between S in the mixed layer and salinity 10 m below the MLD. As in Stevenson and Niiler (1983), the entrainment term w_e is computed as

$$w_e = H\left(\frac{\partial h}{\partial t} + \boldsymbol{v}.\nabla h + w_h\right) \tag{4}$$

where $\partial h/\partial t$ is the rate of the mixed layer change, $\boldsymbol{v}.\nabla h$ is the horizontal velocity at the base of the mixed layer multiplied by the horizontal gradient of the MLD, and w_h is the vertical velocity at the base of the mixed layer. H, the Heaviside unit function, equals zero for a shoaling mixed layer ($\partial h/\partial t < 0$) and equals 1 for a deepening mixed layer ($\partial h/\partial t > 0$) (Delcroix & Henin, 1991; Rao & Sivakumar, 2003). Term R represents the residual from the computation, which includes physical processes that are unresolved in this formulation such as diffusion and diapycnal mixing as well as errors in the calculation of other terms.

3. Results and Discussion

3.1. Climatological Currents

In the western equatorial Indian Ocean (i.e., white box in Figure 1a: 50–70°E, 2°S to 2°N), where westward currents tend to be strongest, westward currents, when present, occur in the upper 50 m (Figure 2c), above an eastward flowing equatorial undercurrent (EUC) located in the thermocline layer (i.e., marked by the 20°

C isotherm; Figure 2c). The relatively shallow westward current maxima are found during boreal winter (January–March) and boreal summer (July–September), at which time the winds are westward over the region (Figures 1 and 2). Notably, the amplitude of westward current maxima is stronger during winter than during summer, although the zonal winds are of similar magnitude during these two seasons (Figure 2a). However, the winds persist for different durations of time during the respective seasons such that their cumulative impact on currents during the winter is stronger. We note that approximately one half of the westward jet events (i.e., 22 out of 45 events, 49%) occur during the winter (November–February) while only 20% of the westward events (i.e., 9 out of 45 events) occur during the summer (June–September). The other 14 events occurred in the various months outside of the winter and summer seasons.

The behavior of the MJO, the main driver of the ISO equatorial wind variability during the winter, is quite different than the BSISO that occurs during the summer. The MJO is much stronger, more enduring, and largely confined to the equatorial waveguide during the winter (Adames et al., 2016). For the BSISO, atmospheric ISV exhibits notable northward propagation that restricts its equatorial impact and is generally weaker (Adames et al., 2016). Thus, the MJO-influenced intraseasonal winds are more persistent with greater fetch, resulting in enhanced equatorial zonal current forcing during winter.

Seasonally, the strongest westward currents occur in February, with amplitude of ~1 m s^{-1} at the equator near 60°E (Figures 1a and 2). While eastward-flowing surface currents occur during the Indian intermonsoon in April–May and October–November, the annual mean zonal current in the upper 50 m of the western Indian Ocean is westward (Figure 2d). At its peak, the volume transport of westward surface zonal currents (approximately −8 Sv; 1Sv = 10^6 m^3 s^{-1}) is almost twice as large as that of the peak eastward surface currents (~4.4 Sv). The mean subsurface currents in the thermocline layer are nearly eastward flowing year-round, with the exception of a brief period in July when they reverse, becoming weakly westward (Figure 2c). The standard deviation of intraseasonal zonal current anomalies demonstrates that the currents are most variable in the upper 50 m (e.g., -0.13 ± 0.33 m s^{-1} at the surface), with the variability weakening with depth (Figure 2d).

3.2. Winds and Currents Time-Frequency Characteristics

We use wavelet analyses to examine the dominant periods of intraseasonal zonal wind and zonal current variability in the western Indian Ocean. Equatorial winds have been previously recognized as the dominant forcing of surface currents in the Indian Ocean (Cane, 1980; Iskandar & McPhaden, 2011; Jensen, 1993). In the western equatorial Indian Ocean, intraseasonal zonal wind power has a maximum at higher frequencies with peak spectral energy at 30–40 days (Figure 3). A secondary maximum located near 70 days is also prominent. When the wavelet time series is composited for each day of the year, wind variability is noted to be a maximum between 30 and 50 days during April–May (Figure 3c). Intraseasonal power is more broadband during October–December, eventually partitioning into distinctive high- and low-frequency bands by January and extending through March (Figure 3c).

For intraseasonal zonal current anomalies in the surface layer of the western Indian Ocean, the dominant energy resides in the lower frequencies of the intraseasonal band (i.e., 120–150 days), while substantial energy is also present in the relatively higher frequencies (i.e., 30–90 days) (Figure 4). Year-to-year variability in the intraseasonal periods is also evident. For example, stronger ISV occurred during 1997, 2008, and 2014 (Figures 4a and 4b). We also note a seasonal dependence of ISV (Figure 4c). At higher frequencies (i.e., periods less than 50 days), substantial power is noted during April–May and October–November, coincident with the intermonsoon periods. At lower frequencies, peak power occurs during February–March, coincident with the timing of strong intraseasonal westward currents in the western equatorial Indian Ocean (Figure 4c).

3.3. Mechanisms of the ISV

Using a time series of box-averaged (see Figure 1a) intraseasonal zonal current anomalies at 50–70°E, 2°S to 2°N as a reference index and lag correlating it against intraseasonal zonal wind anomalies at each longitude along the equator, the strongest correlation between currents and winds (~0.8) occurs between 60°E and 70°E, when the winds lead the currents by ~4–5 days (Figure 2b). This suggests that intraseasonal zonal current variability in the region is primarily locally forced. Weaker positive correlations between the currents and the winds are found to the east and west of this region. The lead time of 4 days is consistent with the

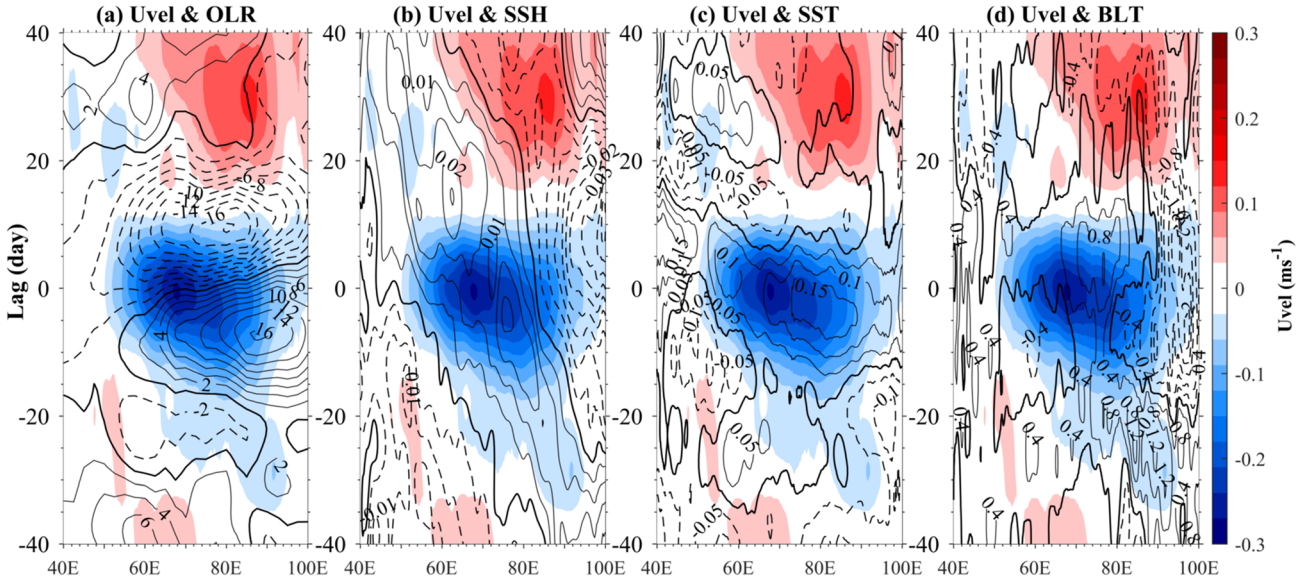

Figure 5. Composites of intraseasonal anomalies of zonal currents averaged from 5°S to 5°N (color shading, m s^{-1}). Contours of intraseasonal (a) outgoing long wave radiation (W m^{-2}), (b) sea surface height (m), (c) sea surface temperature (°C), and (d) barrier layer thickness (m) anomalies are overlaid. Only the 22 boreal winter and 9 boreal summer westward current events are used to make these composites.

results of Rao et al. (2017), which suggests that it takes approximately 4–5 days for surface zonal currents in the equatorial Indian Ocean to respond to wind momentum that is trapped in the mixed layer.

Using composite analyses of westward jet events during boreal winter and boreal summer (i.e., seasons when the jets typically occur), we further examine the causes of the ISV of westward jets in the equatorial Indian Ocean. Intraseasonal westerly winds associated with the suppressed phase of atmospheric intraseasonal convection (i.e., positive OLR anomalies; Figure 5a) occupy the tropical equatorial Indian Ocean during lag −50 to lag −40 days (Figure 6a). These westerly winds drive the eastward surface currents that are present in the equatorial Indian Ocean during lag −50 to lag −40 days (Figures 6a and 6b). Winds in the equatorial region begin to reverse from eastward to westward at lag −30 days (as the OLR anomalies weaken), being strongest in the eastern Indian Ocean and weakest in the western Indian Ocean (Figure 6c). The westward jets are subsequently generated in the eastern Indian Ocean during this time (Figure 6c).

The westward jets reach the central Indian Ocean by lag −20 days, then strengthen, and extend further west between lags −10 and + 10 days, in association with downwelling Rossby waves, a source of remote forcing (i.e., positive SSHA; Figure 5b). At the same time, low-salinity waters in the east are advected toward the central and western equatorial Indian Ocean (Figure 7) concomitant with strengthening of the barrier layer in the region (Figure 5d). The role of advection produced by intraseasonal westward jets is examined in the next section. Barrier layers are intermediate layers that form between the bottom of the salinity-influenced mixed layer and the top of the thermocline (Girishkumar et al., 2011; Lukas & Lindstrom, 1991; Masson et al., 2002). In Figures 5 and 7, the swiftest surface currents tend to occur within the fresher, warmer surface waters. Previous studies (e.g., Han et al., 1999; Masson et al., 2003) have shown that as the mixed layer thins, the barrier layer thickens (i.e., assuming the isothermal layer depth, ITLD does not change; Figure 5d) and traps momentum, strengthening the effects of wind forcing on the surface current acceleration.

Momentum budget estimates (Figure 8) show that acceleration of the intraseasonal westward jets is controlled mainly by the stress and ZPG terms (as shown by the dashed black line in Figure 8), with the stress term leading the ZPG term by ~5 days, consistent with the adjustment of the ocean to wind-forced equatorial wave dynamics (Nagura & McPhaden, 2008; Yuan & Han, 2006). The ZPG term is mostly eastward due to lower SSH in the east and higher SSH in the west during the events (Figure 5b). Acceleration of intraseasonal westward jets is dominated by the stress term, confirming the dominance of atmospheric intraseasonal convection in locally forcing the intraseasonal zonal currents in the equatorial western Indian Ocean. This suggests that forcing from remote mechanisms, such as equatorial Rossby waves, are weak. The tendency for the

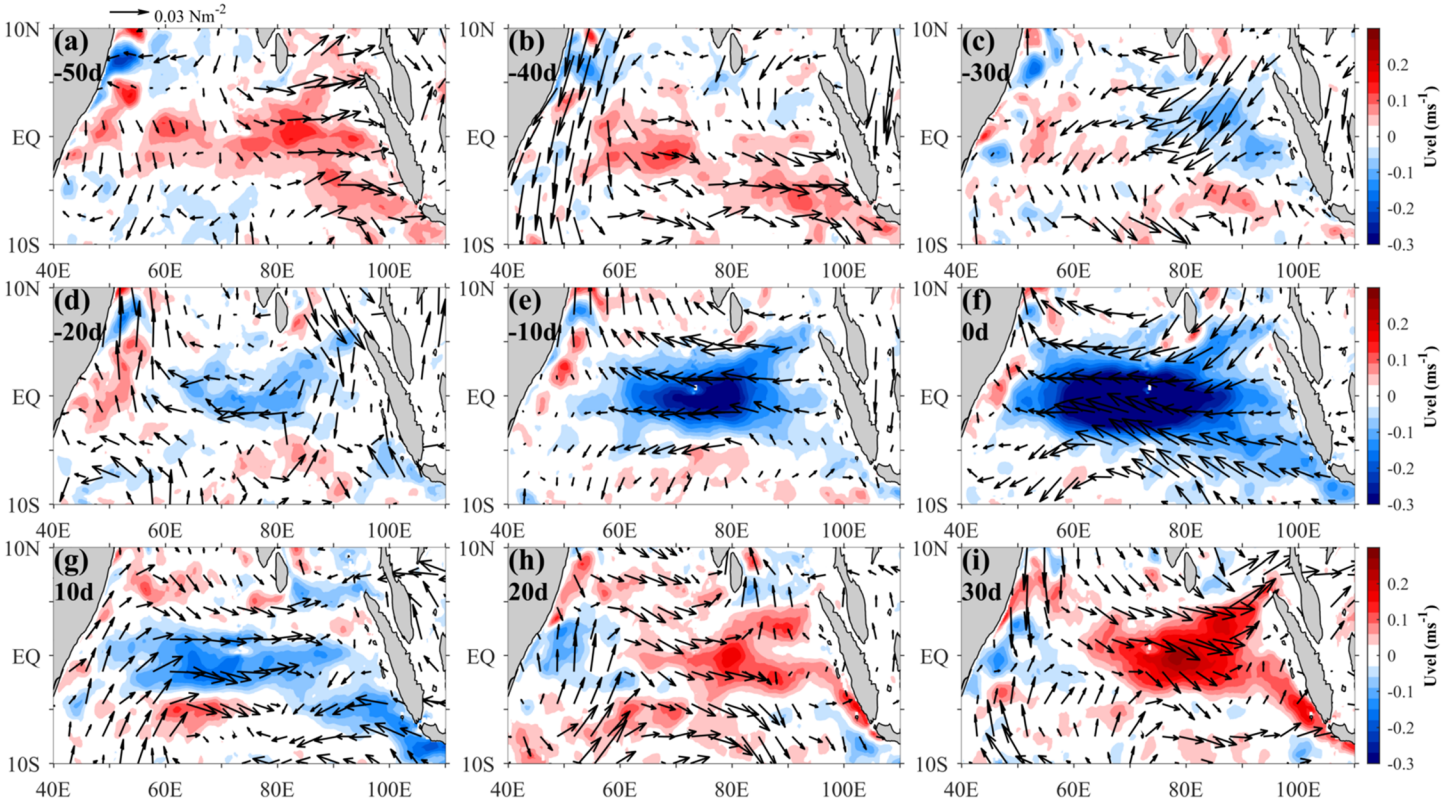

Figure 6. Composites of intraseasonal zonal currents (color shading, m s^{-1}) and wind stress (vectors, N m^{-2}) anomalies during westward current events. Only the 22 boreal winter and 9 boreal summer westward current events are used to make these composites.

intraseasonal westward jet to accelerate occurs when the stress term is westward and greater than the ZPG. Conversely, the tendency for the intraseasonal westward jet to decelerate occurs when the ZPG becomes significant and counteracts the weakening stress term (Figure 8). Contributions from the zonal and meridional momentum advection terms are weak and play nearly negligible roles in the intraseasonal zonal current tendency. On the contrary, the vertical nonlinear momentum advection term tends to have a relatively greater impact on the intraseasonal zonal current acceleration as it mixes the momentum downwards and reinforces the westward wind stress forcing during the event peak days.

At the event peak (i.e., during lag 0 day), westward jets anomalies typically exceed −0.3 m s^{-1} (with a maximum of approximately −0.65 m s^{-1} occurring in May 2008; Figure 4a) and span most of the equatorial Indian Ocean between latitudes ±4° (Figure 6f). By lag +10 days the atmospheric intraseasonal convection is near its peak (Figure 5a), and the westward winds at the equator reverse rapidly (Figure 6g). This phase relationship between intraseasonal convection and wind anomalies is typical for atmospheric intraseasonal convection in the Indian Ocean. The equatorial zonal currents are still westward at this time (Figure 6g), as they require several days to fully adjust to the momentum tendency forcing of the surface winds, as earlier noted. By lag +20 days (Figure 6h), the westward equatorial currents have reversed to be eastward in nearly the entire equatorial region (with only a remnant of westward currents in the west). These sequences of events are consistent with results from previous studies (e.g., Masson et al., 2003; Reppin et al., 1999; Rydbeck et al., 2017; Rydbeck & Jensen, 2017). In summary, the westward surface current anomalies build up slowly but decay rapidly.

3.4. Impact of Westward Jets on Mixed Layer Salinity

The strengthening of the barrier layer in the central equatorial Indian Ocean following the peak of westward jet events was earlier mentioned (Figure 5d). One of the mechanisms for the formation of a barrier layer is the development of a warm, freshwater layer near the surface (Drushka et al., 2014; Lukas &

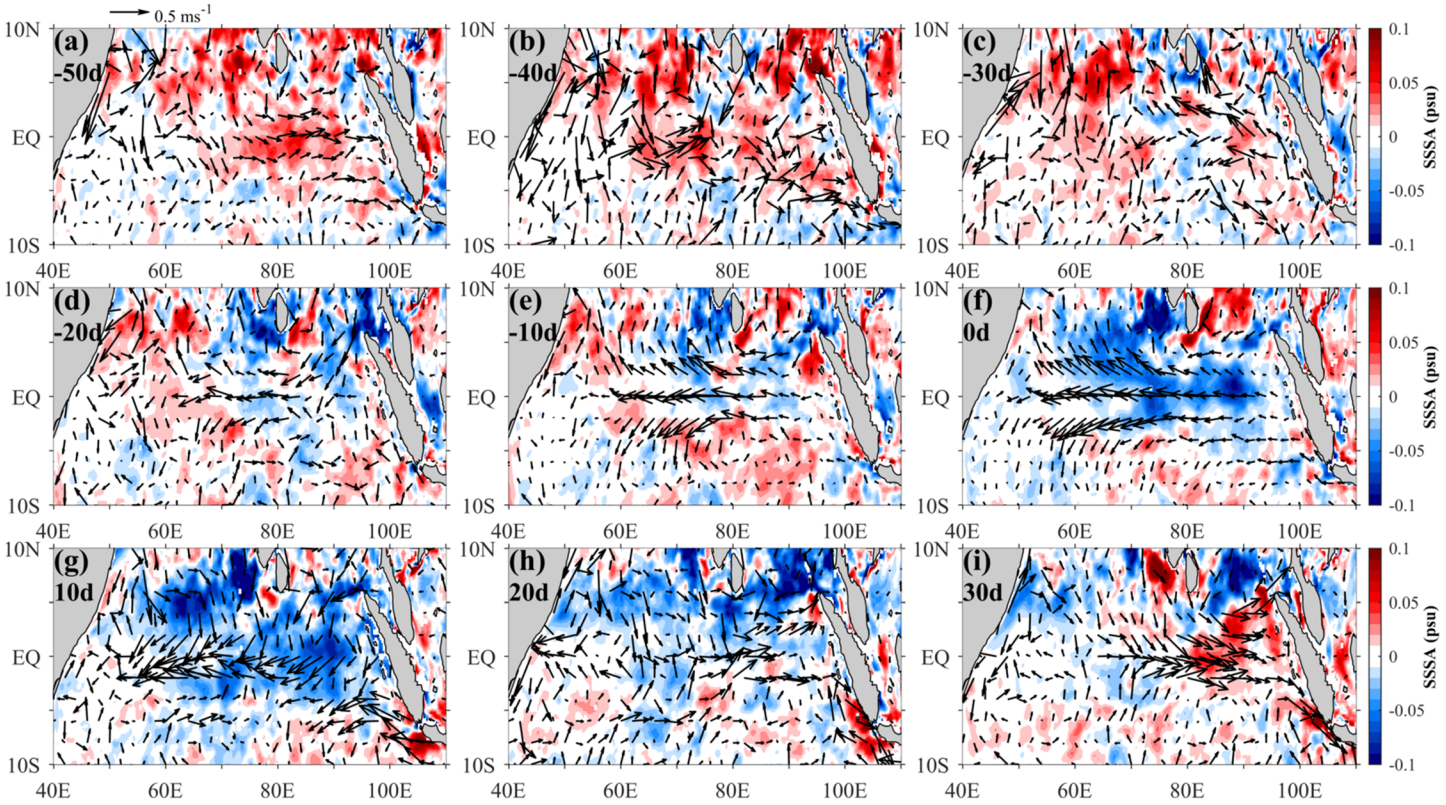

Figure 7. Composites of intraseasonal sea surface salinity (color shading, psu) and surface currents (vectors, m s^{-1}) anomalies during westward current events. Only the 22 boreal winter and 9 boreal summer westward current events are used to make these composites.

Lindstrom, 1991; Masson et al., 2002). In a recent study, Rydbeck et al. (2017) showed that horizontal advection forced by equatorial westward jets associated with Rossby waves resulted in intraseasonal mixed layer warming in the western equatorial Indian Ocean. In this section, we show that westward jets also advect anomalously low-salinity waters from the eastern equatorial Indian Ocean into the central and western equatorial Indian Ocean. In doing so, westward jets modulate the upper ocean stratification.

During lag −50 days to lag −40 days, high salinity waters occupy the equatorial Indian Ocean, being advected by anomalous eastward zonal currents from the high-salinity-dominated western equatorial Indian Ocean to the low-salinity-dominated eastern equatorial Indian Ocean (Figures 7a and 7b). By lag −30 days, the presence of this high-salinity waters in the equatorial Indian Ocean wanes as the anomalous westward currents begin to form in the eastern equatorial Indian Ocean (Figure 7c). Low-salinity waters in the eastern equatorial Indian Ocean originate from the freshwater-dominated Bay of Bengal (Han & McCreary, 2001; Jensen, 2001; Nyadjro et al., 2010; Thompson et al., 2006) and are advected equatorward during lag −20 days (Figure 7d).

Using Equation 3, we quantify the various contributors to the intraseasonal mixed layer salinity tendency in the equatorial western Indian Ocean. Salt budget estimates show that the largest contributor to the intraseasonal freshening of mixed layer salinity in the western equatorial Indian Ocean during the event peak is the westward advection of low-salinity waters. The phase of the mixed layer salinity tendency generally follows that of the zonal advection with a 0.87 correlation between them. The freshening produced by zonal advection begins after lag −35 days (Figure 9a). By lag −10 days the contribution of zonal advection to mixed layer salinity tendency has increased to approximately -2×10^{-3} psu day^{-1}. This is twice as large as the next highest contributor during this time, atmospheric forcing through net freshwater flux that increases the mixed layer salinity (Figure 9a).

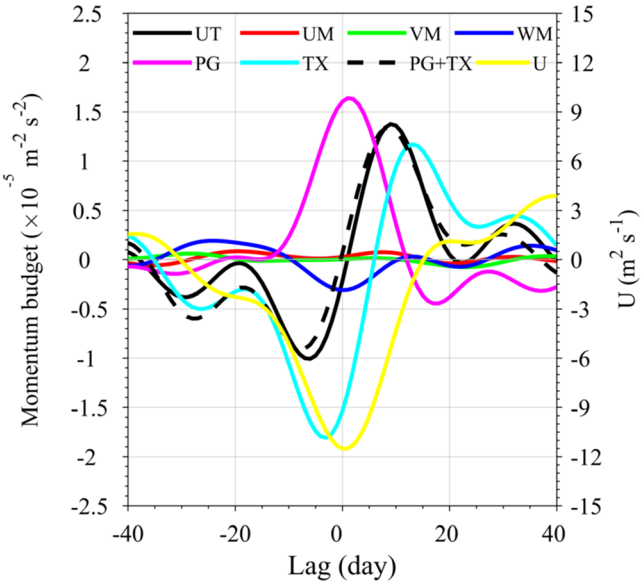

Figure 8. Depth-integrated intraseasonal momentum budget terms averaged over 50–70°E, 1°S to 1°N for zonal acceleration ∂u/∂t (UT, black line), zonal momentum advection (UM, red line), meridional momentum advection (VM, green line), vertical momentum advection (WM, blue line), zonal pressure gradient force (PG, magenta line), surface wind stress (TX, cyan line), and sum of pressure gradient force and surface wind stress (PG + TX, dashed black line). U (yellow line) represents zonal current integrated over the mixed layer. Shear stress at the mixed layer base and horizontal friction terms are negligible and therefore not plotted.

The freshening impact of westward advection on mixed layer salinity reaches its maximum during the event peak contributing approximately -3.5×10^{-3} psu day^{-1} to the mixed layer salinity tendency (Figure 9a). Immediately following the event peak and coinciding with the convective peak of the atmospheric intraseasonal convection (Figure 5a), net freshwater flux tendency reverses, freshening the mixed layer salinity, consistent with results of Drushka et al. (2014) and Grunseich et al. (2011). On the other hand, the tendency from subsurface processes, meridional advection, and unresolved physical processes (i.e., the residual term, *R*) is to counteract this freshening impact and increase the salinity in the mixed layer. The net effect however is a fresher mixed layer due to the overwhelming influence of westward jet-driven salt advection during the event peak. By lag +15 days, the sign of the zonal advection term reverses, which together with a positive net freshwater flux term counteracts the freshening impact by both meridional advection and unresolved processes, such that the mixed layer salinity tendency is positive.

To demonstrate the impactful role of westward jets in the zonal advection term of the salinity budget, we decompose the zonal advection term into its intraseasonal and non-intraseasonal components (Rydbeck et al., 2017). The zonal advection term from Equation 3 can be rewritten as

$$-\left(u\frac{\partial S}{\partial x}\right)' = -\left(u'\frac{\partial S}{\partial x}\right)' - \left((u-u')\frac{\partial S}{\partial x}\right)' \quad (5)$$

where the first term on the right-hand side of Equation 5 represents the advection of salt by intraseasonal zonal currents and the second term represents the advection of salt by non-intraseasonal zonal currents (i.e., currents with periods below 20 days and above 200 days).

When intraseasonal zonal currents are removed from the salt budget (i.e., first term on the right-hand side of Equation 5), the salinity tendency during the peak of the events reverses sign from freshening to salting

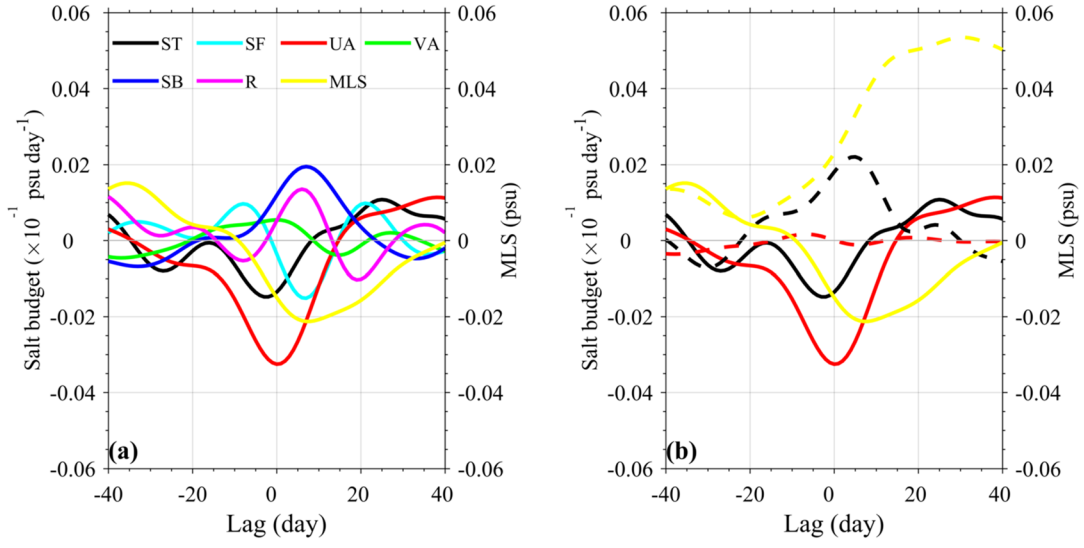

Figure 9. Intraseasonal mixed layer salt budget terms averaged over 50–70°E, 5°S to 5°N for salinity tendency ∂S/∂t (ST, black line), surface freshwater forcing (SF, cyan line), zonal component of advection (UA, red line), meridional component of advection (VA, green line), subsurface influence (SB, blue line), and residuals (R, magenta line). MLS (yellow line) represents salinity averaged over the mixed layer. In Figure 9a, all the terms in Equation 3 are shown. In Figure 9b, horizontal advection by intraseasonal zonal currents is removed from the salinity tendency (black line), zonal component of advection (red line), and the MLS (yellow line) and is shown in dashed lines. The corresponding complete terms from Figure 9a are repeated in Figure 9b.

(Figure 9b). While the salinity tendency that includes the intraseasonal zonal currents peaked at lag −2 days, the salinity tendency with the intraseasonal zonal currents removed, peaked at lag +4 days. Without the inclusion of intraseasonal zonal currents, the zonal advective term is nearly zero, and the mixed layer salinity anomaly becomes much saltier (i.e., from −0.02 to +0.055 psu) and reaches its maximum several days after the peak of the events. This result emphasizes the important freshening role of westward jets in the western Indian Ocean.

4. Summary and Conclusion

Westward jets transport heat and salt from the eastern Indian Ocean into the central and western Indian Ocean, which impacts air-sea interactions, particularly on intraseasonal timescales (Cane, 1980; Rydbeck et al., 2017; Rydbeck & Jensen, 2017; Webber et al., 2010). Consequently, it is worthwhile to understand the occurrence and ISV of westward currents in the equatorial Indian Ocean. Our results show that the volume transport associated with westward currents during boreal winter is greater than that during boreal summer, as the surface wind forcings tend to persist for longer periods during winter.

By defining an index for intraseasonal westward jet events, we are able to formulate composites of their salient features and analyze their behavior. The amplitude of westward jets is strongest during the boreal winter with a peak amplitude of ~1 m s^{-1}. Composite analyses reveal that the excitation and maintenance of intense westward equatorial jets within the equatorial Indian Ocean are primarily locally forced by atmospheric intraseasonal convection-driven wind anomalies. Upon propagating from the central to the western equatorial Indian Ocean, atmospheric ISOs (e.g., MJO) develop in the western Indian Ocean. The rapid reversal of surface wind anomalies following the passage of the active phase of atmospheric intraseasonal convection results in a dramatic and rapid termination of westward jets. A momentum budget estimate confirms the dominant role of intraseasonal winds as it shows significant contributions from intraseasonal wind stress and ZPG terms, with westward intraseasonal wind stress aiding the westward acceleration of intraseasonal jets in the equatorial Indian Ocean. Eastward ZPG then acts to counteract this impact, causing a deceleration and eventual reversal of the intraseasonal westward jets.

The westward jets are associated with a warming and freshening of the equatorial Indian Ocean basin. Using an intraseasonal salt budget, we demonstrate that zonal advection by westward jets are largely responsible for the freshening in the central and western Indian Ocean. When the westward jet is removed from the budget estimations, the zonal advection term becomes near zero, and the mixed layer becomes saltier. Likewise, Rydbeck et al. (2017) showed that Rossby waves and westward jets along the equatorial Indian Ocean caused a warming of ~0.12–0.15°C in the western equatorial Indian Ocean. Subsequently, these warm, fresh waters lead to a thickening of the barrier layer in the western equatorial Indian Ocean. As the barrier layer thickens, the water column becomes more stratified and inhibits mixing between the surface mixed layer and the thermocline (McPhaden & Foltz, 2013). Such variations in the barrier layer thickness have impacts on the coupled ocean-atmosphere system. Future work will aim to understand whether the atmospheric intraseasonal convective forcing of westward jets may ultimately feedback onto the atmospheric intraseasonal convection itself through variations of sea surface temperature, salinity, and ocean stratification.

Data Availability Statement

The output is freely available from the data repository of the HYCOM Consortium at (ftp://ftp.hycom.org/datasets/GLBb0.08/expt_53.X/). OLR data are obtained from NOAA (http://www.esrl.noaa.gov/psd/). ECMWF winds data are downloaded online (from https://www.ecmwf.int/en/forecasts/datasets).

Acknowledgments

This work was supported in part by the Office of Naval Research (ONR) through the Earth Systems Prediction Capability and in part by the ONR-Direct Research Initiatives, "Northern Arabian Sea Circulation autonomous research (NASCar)" project under Grant 73-4347-34-5, and "Oceanic Control of Monsoon Intra-Seasonal Oscillations in the Tropical Indian Ocean and the Bay of Bengal (MISO-BoB)" project under Grant 73-4347-27-5. The reanalysis outputs are from HYCOM experiment 53X run by the Naval Research Laboratory, Stennis Space Center, MS, USA. Thanks to Dr. David Wang for helping with some aspects of the data analysis. We thank the anonymous reviewers whose comments helped improve the manuscript.

References

Adames, A. F., Wallace, J. M., & Monteiro, J. M. (2016). Seasonality of the structure and propagation characteristics of the MJO. *Journal of the Atmospheric Sciences*, *73*(9), 3511–3526. https://doi.org/10.1175/JAS-D-15-0232.1

Cane, M. (1980). On the dynamics of equatorial currents, with application to the Indian Ocean. *Deap Sea Research Part A Oceanographic Research Papers*, *27*(7), 525–544. https://doi.org/10.1016/0198-0149(80)90038-2

Canuto, V. M., Howard, A., Cheng, Y., & Dubovikov, M. S. (2001). Ocean turbulence. Part I: One-point closure model. Momentum and heat vertical diffusivities. *Journal of Physical Oceanography*, *31*(6), 1413–1426. https://doi.org/10.1175/1520-0485(2001)031<1413:OTPIOP>2.0.CO;2

Canuto, V. M., Howard, A., Cheng, Y., & Dubovikov, M. S. (2002). Ocean turbulence. Part II: Vertical diffusivities of momentum, heat, salt, mass, and passive scalars. *Journal of Physical Oceanography*, *32*(1), 240–264. https://doi.org/10.1175/1520-0485(2002)032<0240:OTPIVD>2.0.CO;2

Chowdary, J. S., Gnanaseelan, C., & Xie, S. P. (2009). Westward propagation of barrier layer formation in the 2006–07 Rossby wave event over the tropical southwest Indian Ocean. *Geophysical Research Letters*, *36*, L04607. https://doi.org/10.1029/2008GL036642

Cummings, J. A. (2005). Operational multivariate ocean data assimilation. *Quarterly Journal of the Royal Meteorological Society*, *131*(613), 3583–3604. https://doi.org/10.1256/qj.05.105

D'Addezio, J. M., & Subrahmanyam, B. (2016). Role of salinity on the interannual variability of the Seychelles-Chagos thermocline ridge. *Remote Sensing of Environment*, *180*, 178–192. https://doi.org/10.1016/j.rse.2016.02.051

de Boyer Montégut, C., Madec, G., Fischer, A. S., Lazar, A., & Iudicone, D. (2004). Mixed layer depth over the global ocean: An examination of profile data and a profile-based climatology. *Journal of Geophysical Research*, *109*, C12003. https://doi.org/10.1029/2004JC002378

Dee, D. P., Uppala, S. M., Simmons, A. J., Berrisford, P., Poli, P., Kobayashi, S., et al. (2011). The ERA-Interim reanalysis: Configuration and performance of the data assimilation system. *Quarterly Journal of the Royal Meteorological Society*, *137*(656), 553–597. https://doi.org/10.1002/qj.828

Delcroix, T., & Henin, C. (1991). Seasonal and Interannual variations of the sea surface salinity in the tropical Pacific Ocean. *Journal of Geophysical Research*, *96*, 22,135–22,150. https://doi.org/10.1029/91JC02124

Delcroix, T., Picaut, J., & Eldin, G. (1991). Equatorial Kelvin and Rossby waves evidence in the Pacific Ocean through Geosat sea level and surface current anomalies. *Journal of Geophysical Research*, *96*(S01), 3249–3262. https://doi.org/10.1029/90JC01758

DeMott, C. A., Klingaman, N. P., & Woolnough, S. J. (2015). Atmosphere-ocean coupled processes in the Madden-Julian Oscillation. *Reviews of Geophysics*, *53*, 1099–1154. https://doi.org/10.1002/2014RG000478

Deshpande, A., Gnanaseelan, C., Chowdary, J. S., & Rahul, S. (2017). Interannual spring Wyrtki jet variability and its regional impacts. *Dynamics of Atmospheres and Oceans*, *78*, 26–37. https://doi.org/10.1016/j.dynatmoce.2017.02.001

Drenkard, E. J., & Karnauskas, K. B. (2014). Strengthening of the Pacific Equatorial Undercurrent in the SODA reanalysis: Mechanisms, ocean dynamics, and implications. *Journal of Climate*, *27*(6), 2405–2416. https://doi.org/10.1175/JCLI-D-13-00359.1

Drushka, K., Sprintall, J., & Gille, S. T. (2014). Subseasonal variations in salinity and barrier- layer thickness in the eastern equatorial Indian Ocean. *Journal of Geophysical Research: Oceans*, *119*, 805–823. https://doi.org/10.1002/2013JC009422

Girishkumar, M. S., Ravichandran, M., McPhaden, M. J., & Rao, R. R. (2011). Intraseasonal variability in barrier layer thickness in the south-central Bay of Bengal. *Journal of Geophysical Research*, *116*, C03009. https://doi.org/10.1029/2010JC006657

Gnanaseelan, C., Deshpande, A., & McPhaden, M. J. (2012). Impact of Indian Ocean Dipole and El Niño/Southern Oscillation wind-forcing on the Wyrtki jets. *Journal of Geophysical Research*, *117*, C08005. https://doi.org/10.1029/2012JC007918

Grunseich, G., Subrahmanyam, B., & Arguez, A. (2011). Influence of the Madden-Julian Oscillation on sea surface salinity in the Indian Ocean. *Geophysical Research Letters*, *38*, L17605. https://doi.org/10.1029/2011GL049047

Grunseich, G., Subrahmanyam, B., & Wang, B. (2013). The Madden-Julian Oscillation detected in Aquarius salinity observations. *Geophysical Research Letters*, *40*, 5461–5466. https://doi.org/10.1002/2013GL058173

Halliwell, G. R. (2004). Evaluation of vertical coordinate and vertical mixing algorithms in the HYbrid Coordinate Ocean Mode (HYCOM). *Ocean Modelling*, *7*(3-4), 285–322. https://doi.org/10.1016/j.ocemod.2003.10.002

Han, W., & McCreary, J. P. (2001). Modeling salinity distributions in the Indian Ocean. *Journal of Geophysical Research*, *106*(C1), 859–877. https://doi.org/10.1029/2000JC000316

Han, W., McCreary, J. P., Anderson, D. L. T., & Mariano, A. J. (1999). Dynamics of the eastern surface jets in the equatorial Indian Ocean. *Journal of Physical Oceanography*, *29*(9), 2191–2209. https://doi.org/10.1175/1520-0485(1999)029<2191:DOTESJ>2.0.CO;2

Hendon, H. H., Zhang, C., & Glick, J. (1999). Interannual fluctuations of the Madden-Julian Oscillation during austral summer. *Journal of Climate*, *12*, 2538–2550. https://doi.org/10.1175/1520-0442(1999)012<2,538:IVOTMJ>2.0.CO;2

Hermes, J. C., & Reason, C. J. C. (2008). Annual cycle of the South Indian Ocean (Seychelles- Chagos) thermocline ridge in a regional ocean model. *Journal of Geophysical Research*, *107*, C04035. https://doi.org/10.1029/2007JC004363

IOC, IHO, & BODC (2003). Centenary Edition of the General Bathymetric Chart of the Oceans (GEBCO) Digital Atlas. *British Oceanographic Data Centre, Natural Environmental Research Council, Liverpool*.

Iskandar, I., & McPhaden, M. J. (2011). Dynamics of wind-forced intraseasonal zonal current variations in the equatorial Indian Ocean. *Journal of Geophysical Research*, *116*, C06019. https://doi.org/10.1029/2010JC006864

Jensen, T. G. (1993). Equatorial variability and resonance in a wind-driven Indian Ocean model. *Journal of Geophysical Research*, *98*(C12), 22,533–22,552. https://doi.org/10.1029/93JC02565

Jensen, T. G. (2001). Arabian Sea and Bay of Bengal exchange of salt and tracers in an ocean model. *Geophysical Research Letters*, *28*(20), 3967–3970. https://doi.org/10.1029/2001GL013422

Joseph, S., Wallcraft, A. J., Jensen, T. G., Ravichandran, M., Shenoi, S. S. C., & Nayak, S. (2012). Weakening of spring Wyrtki jets in the Indian Ocean during 2006–2011. *Journal of Geophysical Research*, *117*, C04012. https://doi.org/10.1029/2011JC007581

Knox, R. A. (1976). On a long series of measurements of Indian Ocean equatorial currents near Addu Atoll. *Deep Sea Research and Oceanographic Abstracts*, *23*(3), 211–221. https://doi.org/10.1016/0011-7471(76)91325-5

Li, Y., Han, W., & Lee, T. (2015). Intraseasonal sea surface salinity variability in the equatorial Indo-Pacific Ocean induced by Madden-Julian Oscillations. *Journal of Geophysical Research: Oceans*, *120*, 2233–2258. https://doi.org/10.1002/2014JC010647

Liao, X., Du, Y., Zhan, H., Wang, T., & Feng, M. (2017). Wintertime phytoplankton blooms in the Western Equatorial Indian Ocean associated with the Madden-Julian Oscillation. *Journal of Geophysical Research: Oceans*, *122*, 9855–9869. https://doi.org/10.1002/2017JC013203

Liebmann, B., & Smith, C. A. (1996). Description of a complete (interpolated) outgoing longwave radiation dataset. *Bulletin of the American Meteorological Society*, *77*, 1275–1277.

Lukas, R., & Lindstrom, E. (1991). The mixed layer of the western equatorial Pacific Ocean. *Journal of Geophysical Research*, *96*(S01), 3343–3357. https://doi.org/10.1029/90JC01951

Luyten, J. R., & Roemmich, D. H. (1982). Equatorial currents at semiannual period in the Indian Ocean. *Journal of Physical Oceanography*, *12*(5), 406–413. https://doi.org/10.1175/1520-0485(1982)012<0406:ECASAP>2.0.CO;2

Madden, R. A., & Julian, P. R. (1971). Detection of a 40–50-day oscillation in the zonal wind in the tropical Pacific. *Journal of the Atmospheric Sciences*, *28*(5), 702–708. https://doi.org/10.1175/1520-0469(1971)028<0702:DOADOI>2.0.CO;2

Masson, S., Delecluse, P., Boulanger, J.-P., & Menkes, C. (2002). A model study of the seasonal variability and formation mechanisms of barrier layer in the eastern equatorial Indian Ocean. *Journal of Geophysical Research*, *107*(C12), 8017. https://doi.org/10.1029/2001JC000832

Masson, S., Menkes, C., Delecluse, P., & Boulanger, J.-P. (2003). Impacts of salinity on the eastern Indian Ocean during the termination of the fall Wyrtki Jet. *Journal of Geophysical Research*, *108*(C3), 3067. https://doi.org/10.1029/2001JC000833

Matthews, A. J., Singhruck, P., & Heywood, K. J. (2010). Ocean temperature and salinity components of the Madden-Julian Oscillation observed by Argo floats. *Climate Dynamics*, *35*(7-8), 1149–1168. https://doi.org/10.1007/s00382-009-0631-7

McCreary, J. P., Murtugudde, R., Vialard, J., Vinayachandran, P. N., Wiggert, J. D., Hood, R. R., et al. (2009). Biophysical processes in the Indian Ocean. In J. D. Wiggert, et al. (Eds.), *Indian Ocean biogeochemical processes and ecological variability* (pp. 9–32). Washington, DC: American Geophysical Union. https://doi.org/10.1029/2008GM000768

McPhaden, M. J., & Foltz, G. R. (2013). Intraseasonal variations in the surface layer heat balance of the central equatorial Indian Ocean: The importance of zonal advection and vertical mixing. *Geophysical Research Letters*, *40*, 2737–2741. https://doi.org/10.1002/grl.50536

McPhaden, M. J., Wang, Y., & Ravichandran, M. (2015). Volume transports of the Wyrtki jets and their relationship to the Indian Ocean Dipole. *Journal of Geophysical Research: Oceans*, *120*, 5302–5317. https://doi.org/10.1002/2015JC010901

Metzger, E. J., Helber, R. W., Hogan, P. J., Posey, P. G., Thoppil, P. G., Townsend, T. L., et al. (2017). Global Ocean Forecast System 3.1 validation testing. Naval Research Laboratory Technical Report. Retrieved from http://www.dtic.mil/docs/citations/AD1034517

Nagura, M., & McPhaden, M. J. (2008). The dynamics of zonal current variations in the central equatorial Indian Ocean. *Geophysical Research Letters*, *35*, L23603. https://doi.org/10.1029/2008GL035961

Nagura, M., & McPhaden, M. J. (2010). Wyrtki Jet dynamics: Seasonal variability. *Journal of Geophysical Research*, *115*, C07009. https://doi.org/10.1029/2009JC005922

Nagura, M., & McPhaden, M. J. (2014). Zonal momentum budget along the equator in the Indian Ocean from a high-resolution ocean general circulation model. *Journal of Geophysical Research: Oceans*, *119*, 4444–4461. https://doi.org/10.1002/2014JC009895

Nyadjro, E. S., Jensen, T. G., Richman, J. G., & Shriver, J. F. (2017). On the relationship between wind, SST and the thermocline in the Seychelles-Chagos Thermocline Ridge. *IEEE Geoscience and Remote Sensing Letters*, *14*(12), 2315–2319. https://doi.org/10.1109/LGRS.2017.2762961

Nyadjro, E. S., & McPhaden, M. J. (2014). Variability of zonal currents in the eastern equatorial Indian Ocean on seasonal to interannual time scales. *Journal of Geophysical Research: Oceans*, *119*, 7969–7986. https://doi.org/10.1002/2014JC010380

Nyadjro, E. S., Subrahmanyam, B., Murty, V. S. N., & Shriver, J. F. (2010). Salt transport in the near-surface layer in the monsoon-influenced Indian Ocean using HYCOM. *Geophysical Research Letters*, *37*, L15603. https://doi.org/10.1029/2010GL044127

Qiao, L., & Weisberg, R. H. (1997). The zonal momentum balance of the equatorial undercurrent in the central Pacific. *Journal of Physical Oceanography*, *27*(6), 1094–1119.

Qiu, Y., Li, L., & Yu, W. (2009). Behavior of the Wyrtki Jet observed with surface drifting buoys and satellite altimeter. *Geophysical Research Letters*, *36*, L18607. https://doi.org/10.1029/2009GL039120

Rao, R. R., Horii, T., Masumoto, Y., & Mizumo, K. (2017). Observed variability in the upper layers at the equator, 90E in the Indian Ocean during 2001–2008, 1: Zonal currents. *Climate Dynamics*, *49*, 1077–1105. https://doi.org/10.1007/s00382-016-3234-0

Rao, R. R., Molinari, R. L., & Fiesta, J. F. (1989). Evolution of the climatological near-surface thermal structure of the tropical Indian Ocean: 1. Description of mean monthly mixed layer depth, and sea surface temperature, surface current, and surface meteorological fields. *Journal of Geophysical Research*, *94*(C8), 10,801–10,815. https://doi.org/10.1029/JC094iC08p10801

Rao, R. R., & Sivakumar, R. (2003). Seasonal variability of sea surface salinity and salt budget of the mixed layer of the north Indian Ocean. *Journal of Geophysical Research*, *108*(C1), 3009. https://doi.org/10.1029/2001JC000907

Reppin, J., Schott, F. A., Fisher, J., & Quadfasel, D. (1999). Equatorial currents and transports in the upper central Indian Ocean: Annual cycle and interannual variability. *Journal of Geophysical Research*, *104*(C7), 15,495–15,514. https://doi.org/10.1029/1999JC900093

Rydbeck, A. V., & Jensen, T. G. (2017). Oceanic impetus for convective onset of the Madden- Julian Oscillation in the western Indian Ocean. *Journal of Climate*, *30*(11), 4299–4316. https://doi.org/10.1175/JCLI-D-16-0595.1

Rydbeck, A. V., Jensen, T. G., & Nyadjro, E. S. (2017). Intraseasonal sea surface warming in the western Indian Ocean by oceanic equatorial Rossby waves. *Geophysical Research Letters*, *44*, 4224–4232. https://doi.org/10.1002/2017GL073331

Saha, S., Moorthi, S., Pan, H. L., Wu, X., Wang, J., Nadiga, S., et al. (2010). The NCEP climate forecast system reanalysis. *Bulletin of the American Meteorological Society*, *91*(8), 1015–1058. https://doi.org/10.1175/2010BAMS3001.1

Senan, R., Sengupta, D., & Goswami, B. N. (2003). Intraseasonal "monsoon jets" in the equatorial Indian Ocean. *Geophysical Research Letters*, *30*(14), 1750. https://doi.org/10.1029/2003GL017583

Sengupta, D., Senan, R., & Goswami, B. N. (2001). Origin of intraseasonal variability of circulation in the tropical central Indian Ocean. *Geophysical Research Letters*, *28*, 1267–1270. https://doi.org/10.1029/2000GL012251

Stevenson, J. W., & Niiler, P. P. (1983). Upper ocean heat budget during the Hawaii-to-Tahiti shuttle experiment. *Journal of Physical Oceanography*, *13*(10), 1894–1907. https://doi.org/10.1175/1520-0485(1983)013<1894:UOHBDT>2.0.CO;2

Thompson, B., Gnanaseelan, C., & Salvekar, P. S. (2006). Variability in the Indian Ocean circulation and salinity and its impact on SST anomalies during dipole events. *Journal of Marine Research*, *64*(6), 853–880. https://doi.org/10.1357/002224006779698350

Trenary, L. L., & Han, W. (2012). Intraseasonal-to-interannual variability of south Indian Ocean sea level and thermocline: Remote versus local forcing. *Journal of Physical Oceanography*, *42*(4), 602–627. https://doi.org/10.1175/JPO-D-11-084.1

Wallcraft, A. J., Kara, A. B., & Hurlburt, H. E. (2005). Convergence of Laplacian diffusion versus resolution of an ocean model. *Geophysical Research Letters*, *32*(L07604). https://doi.org/10.1029/2005GL022514

Webber, B. G. M., Matthews, A. J., & Heywood, K. J. (2010). A dynamical ocean feedback mechanism for the Madden-Julian Oscillation. *Quarterly Journal of the Royal Meteorological Society*, *136*, 740–754. https://doi.org/10.1002/qj.604

Weisberg, R. H., & Wang, C. (1997). Slow variability in the equatorial west-central Pacific in relation to ENSO. *Journal of Climate*, *10*(8), 1998–2017. https://doi.org/10.1175/1520-0442(1997)010<1998:SVITEW>2.0.CO;2

Wyrtki, K. (1973). An equatorial jet in the Indian Ocean. *Science*, *181*(4096), 262–264. https://doi.org/10.1126/science.181.4096.262

Yoshida, K. (1959). A theory of the Cromwell current (the equatorial undercurrent) and of the equatorial upwelling—An interpretation in a similarity to a coastal circulation. *Journal of the Oceanographic Society of Japan*, *15*(4), 159–170. https://doi.org/10.5928/kaiyou1942.15.159

Yuan, D., & Han, W. (2006). Roles of equatorial waves and western boundary reflection in the seasonal circulation of the equatorial Indian Ocean. *Journal of Physical Oceanography*, *36*(5), 930–944. https://doi.org/10.1175/JPO2905.1